

Near- to mid-infrared spectroscopy of the heavily obscured AGN LEDA 1712304 with AKARI/IRC

T. Tsuchikawa,¹ H. Kaneda,¹ S. Oyabu,¹ T. Kokusho,¹ K. Morihana,¹ H. Kobayashi,¹
M. Yamagishi² and Y. Toba^{3,4,5}

¹ Graduate School of Science, Nagoya University, Furo-cho, Chikusa-ku, Nagoya, Aichi 464-8602, Japan
e-mail: tsuchikawa@u.phys.nagoya-u.ac.jp

² Institute of Space and Astronautical Science, Japan Aerospace Exploration Agency, 3-1-1 Yoshinodai, Chuo-ku, Sagami-hara, Kanagawa, 252-5210, Japan

³ Department of Astronomy, Kyoto University, Kitashirakawa-Oiwake-cho, Sakyo-ku, Kyoto 606-8502, Japan

⁴ Academia Sinica Institute of Astronomy and Astrophysics, 11F of Astronomy-Mathematics Building, AS/NTU, No.1, Section 4, Roosevelt Road, Taipei 10617, Taiwan

⁵ Research Center for Space and Cosmic Evolution, Ehime University, 2-5 Bunkyo-cho, Matsuyama, Ehime 790-8577, Japan

Received ** ***, 2019; accepted ** ***, 2019

ABSTRACT

Context. Although heavily obscured active galactic nuclei (AGNs) have been found by many observational studies, the properties of the surrounding dust are poorly understood. Using AKARI/IRC spectroscopy, we discover a new sample of a heavily obscured AGN in LEDA 1712304 which shows a deep spectral absorption feature due to silicate dust.

Aims. We study the infrared (IR) spectral properties of circumnuclear silicate dust in LEDA 1712304.

Methods. We perform IR spectral fitting, considering silicate dust properties such as composition, porosity, size and crystallinity. Spectral energy distribution (SED) fitting is also performed to the flux densities in the UV to sub-millimeter range to investigate the global spectral properties.

Results. The best-fit model indicates 0.1 μm -sized porous amorphous olivine ($\text{Mg}_{2x}\text{Fe}_{2-2x}\text{SiO}_4$; $x = 0.4$) with 4% crystalline pyroxene. The optical depth is $\tau_{\text{sil}} \sim 2.3$, while the total IR luminosity and stellar mass are estimated to be $L_{\text{IR}} = (5 \pm 1) \times 10^{10} L_{\odot}$ and $M_{\text{star}} = (2.7 \pm 0.8) \times 10^9 M_{\odot}$, respectively. In such low L_{IR} and M_{star} ranges, there are few galaxies which show that large τ_{sil} .

Conclusions. The silicate dust in the AGN torus of LEDA 1712304 has properties notably similar to those in other AGNs as a whole, but slightly different in the wing shape of the absorption profile. The porosity of the silicate dust suggests dust coagulation or processing in the circumnuclear environments, while the crystallinity suggests that the silicate dust is relatively fresh.

Key words. Infrared: galaxies – galaxies: nuclei – galaxies: individual: LEDA 1712304

1. Introduction

Dust plays an important role in probing the activity of active galactic nuclei (AGN). The AGN unified model (e.g., Antonucci 1993; Urry & Padovani 1995) concludes that a supermassive black hole (SMBH) and its accretion disk are enshrouded by an optically thick dusty torus which has an axisymmetric structure to explain the difference in the optical line profiles. Heavily obscured AGNs which show almost no optical sign of AGN activities have been found by many observational studies (e.g., Sanders & Mirabel 1996; Lutz et al. 1998; Dey et al. 2008; Imanishi et al. 2008; Oyabu et al. 2011). Due to the presence of thick dust layers around the AGN core, the UV and optical emission from the AGN accretion disk is strongly suppressed, and thus AGN identification on the basis of the optical line ratios encounters difficulty for the heavily obscured AGNs. Infrared (IR) observations can identify AGNs without suffering severe dust extinction. For heavily obscured AGNs, the near- to mid-IR range is dominated by the hot dust emission heated by AGNs, where the spectra show power-law like continua. While the presence of heavily obscured AGNs is suggested in many cases, the properties of the surrounding dust, such as size, chemical composition and crystallinity, are poorly understood.

The spectroscopy in the near- to mid-IR range which contains various dust spectral features is effective to understand the properties of dust. In particular, the profiles of the silicate features at around 9.7 μm (Si–O stretching mode) and 18 μm (O–Si–O bending mode) reflect the chemical composition, size distribution, crystallinity and structure of the silicate dust. The silicate features for nearby luminous IR galaxies (LIRGs) and ultra-luminous IR galaxies (ULIRGs) have been studied extensively by *Spitzer*/IRS (e.g., Imanishi 2009; Stierwalt et al. 2013). In particular, many U/LIRGs have deep silicate absorption features (e.g., Roche et al. 1986; Spoon et al. 2007), which tend to possess heavily obscured AGNs (e.g., Imanishi 2009) and are likely to be at the late to final stages of mergers (Stierwalt et al. 2013). On the other hand, the depths of the silicate features in AGNs depend on the AGN type; type-1 Seyferts show the features in either emission or weak absorption, while type-2 Seyferts show those only in absorption (Hao et al. 2007). As a global trend, the number of galaxies which have deep silicate absorption features increases with the IR luminosities of their host galaxies (Imanishi 2009). Spoon et al. (2007) suggested that the difference in the silicate absorption depth depends on the circumnuclear distribution of the dusty torus. Roche et al. (2015) reported that the silicate absorption profiles of NGC 4418 showed spec-

tral variations depending on the slit aperture size, which suggests the presence of extended dust emission around the nucleus. Although the main compositions of the features are likely to be amorphous olivine, crystalline silicate substructures are also detected from heavily obscured ULIRG nuclei (Spoon et al. 2006; Stierwalt et al. 2014).

In AKARI/IRC slit-less spectroscopic surveys, we serendipitously discover a galaxy which shows a notably deep silicate absorption feature but with a relatively low IR luminosity. The galaxy is a local dust-obscured galaxy, LEDA 1712304 ($z = 0.0645$; Hwang et al. 2013). A galaxy classification of LEDA 1712304 based on the optical line ratios is “undetermined” (Hwang et al. 2013), which indicates that the dust extinction in the galaxy is too large to detect optical lines such as [OIII] 5007. On the other hand, the galaxy is expected to possess an AGN hidden in the galactic center based on the result of IR spectral energy distribution (SED) fitting (Hwang et al. 2013). In this paper, we study the spectral properties of silicate dust in LEDA 1712304, using the AKARI/IRC spectroscopic data as well as the photometric data in the UV to submillimeter range. Throughout the paper, we adopt 289.7 Mpc for the distance to the galaxy, assuming the cosmological parameters $H_0 = 70 \text{ km s}^{-1} \text{ Mpc}^{-1}$, $\Omega_\Lambda = 0.7$ and $\Omega_m = 0.3$.

2. Observations

2.1. AKARI IR spectroscopy

LEDA 1712304 was detected serendipitously within the field-of-view of slit-less spectroscopy at 2.5–12.5 μm using InfraRed Camera (IRC; Onaka et al. 2007) onboard the AKARI satellite (Murakami et al. 2007), the mid-IR spectrum of which is among those in the catalog of (Yamagishi et al. 2019). The primary target was IC 860 and the observation was carried out on July 28 2007 with the IRC spectroscopic mode of the astronomical observation template 04 (AOT04) in the framework of the mission program AGNUL (Evolution of ULIRGs and AGNs; PI: T. Nakagawa). In this study, the near-IR spectrum is combined with the mid-IR spectra to create the 2.5–12.5 μm of LEDA 1712304, where three spectroscopic modules were used; the NIR prism (NP) and the two MIR-S grisms (SG1, SG2) covering the wavelength ranges of 1.8–5.5 μm , 4.6–9.2 μm and 7.2–13.4 μm , respectively. The wavelength resolution, $R (= \lambda/\delta\lambda)$, is typically 19 at 3.5 μm , 53 at 6.6 μm and 50 at 10.6 μm for NP, SG1 and SG2, respectively (Ohya et al. 2007). Since LEDA 1712304 was observed with the slit-less spectroscopy, the spectrum does not need to be corrected for the slit loss. The spectra are processed with the data reduction package “IRC Spectroscopy Toolkit Version 20181203”. For extraction of the spectrum, we applied the aperture sizes of 5 pixels (7.3”), 7 pixels (16.4”) and 7 pixels (16.4”) for NP, SG1 and SG2, respectively. The NP and SG spectra were calibrated on the basis of the AKARI 3.2 μm and 9 μm photometric flux densities, respectively. We did not use the spectral regions of 2.0–2.5 μm and 5.0–5.5 μm , which correspond to the edges of the NP spectral coverage, since systematic errors are relatively large in those regions.

2.2. Multi-wavelength photometric data

In order to investigate the global spectral properties of LEDA 1712304, we conducted aperture photometry of the multi-wavelength image data taken with not only AKARI but also *Spitzer* (Fazio et al. 2004; Rieke et al. 2004) and *Herschel*

Table 1. Summary of the aperture radii used for the photometry and the flux densities.

Instrument	aperture radius / [”] ^a	flux density / [mJy]
GALEX NUV	–	0.003 ± 0.001^b
SDSS <i>u</i>	–	0.043 ± 0.005^b
SDSS <i>g</i>	–	0.168 ± 0.003^b
SDSS <i>r</i>	–	0.347 ± 0.003^b
SDSS <i>i</i>	–	0.483 ± 0.004^b
SDSS <i>z</i>	–	0.59 ± 0.02^b
SIRIUS <i>J</i>	12.7	0.90 ± 0.03
SIRIUS <i>H</i>	12.0	1.09 ± 0.03
SIRIUS <i>K_s</i>	12.3	0.90 ± 0.05
IRC 3.2 μm	4.26	2.57 ± 0.06
WISE 3.4 μm	–	2.73 ± 0.06^c
IRAC 3.6 μm	7.06	4.16 ± 0.08
IRAC 4.5 μm	7.32	8.65 ± 0.18
WISE 4.6 μm	–	11.9 ± 0.2^c
IRAC 5.8 μm	8.00	28.8 ± 0.6
IRAC 8.0 μm	8.43	45.3 ± 0.9
IRC 9 μm	–	29 ± 2^d
WISE 12 μm	–	23.7 ± 0.4^c
WISE 22 μm	–	50 ± 2^c
MIPS 24 μm	12.6	50 ± 2
PACS 70 μm	11.5	$(1.8 \pm 0.2) \times 10^2$
PACS 100 μm	14.3	$(3.0 \pm 0.3) \times 10^2$
PACS 160 μm	24.0	< 140
SPIRE 250 μm	37.4	$(5 \pm 1) \times 10^1$
SPIRE 350 μm	50.9	$(4 \pm 1) \times 10^1$

Notes. ^(a) The aperture radii R_{ap} correspond to 3, 10 and $5 \times R_{\text{FWHM}}/2.35$ for SIRIUS, IRAC and the other image data, respectively, where R_{FWHM} is the full width at half maximum (FWHM) of the point spread function (PSF). ^(b) Hwang et al. (2013). ^(c) Cutri et al. (2013). ^(d) Yamagishi et al. (2019).

(Poglitsch et al. 2010; Griffin et al. 2010). The *Spitzer* and *Herschel* image data were retrieved from the *Spitzer* Heritage Archive through the NASA/IPAC IR Science Archive (IRSA) and the ESA *Herschel* science archive, respectively. We applied photometric apertures, R_{ap} , in Table 1, and sky backgrounds were determined in the annuli of inner radii $1.2R_{\text{ap}}$ and outer radii $2R_{\text{ap}}$. We also applied appropriate aperture corrections to the photometric results as mentioned in each of the handbooks. Table 1 summarizes the results of the aperture photometry. LEDA 1712304 was not detected in the *Herschel* 160 μm band with the signal-to-noise ratio (S/N) > 3 . We also observed LEDA 1712304 with Simultaneous Infrared Imager for Unbiased Survey (SIRIUS; Nagashima et al. 1999; Nagayama et al. 2003) on Infrared Survey Facility (IRSF) in South African Astronomical Observatory. SIRIUS has a large field of view ($7' \times 7'$) and enables simultaneous imaging in the *J*, *H* and *K_s* bands. The observation was performed on June 6 2018, and the total integration time was 16.7 minutes. We performed the flux calibration on the basis of the 2MASS Point Source Catalog (Cutri et al. 2003). In addition, we also used the flux densities of LEDA 1712304 taken from the UV, optical and IR catalogs (Hwang et al. 2013; Cutri et al. 2013; Yamagishi et al. 2019).

3. Results

3.1. IR spectral properties

Figure 1 shows the AKARI/IRC 2.5–12.5 μm spectrum of LEDA 1712304. We detect a deep, broad absorption feature due to silicate grains at around 10 μm . We also detect CO ro-vibrational absorption features at around 4.7 μm . Any other spectral features, such as those due to CO₂ ice at 4.27 μm , H₂O ice at 3.05 and 6.02 μm and polycyclic aromatic hydrocarbon (PAH) features at 3.3, 6.2, 7.7 and 11.3 μm , are not detected significantly. The spectrum also shows a steep near-to mid-IR slope, which is likely to indicate that the continuum is dominated by thermal emission of hot dust heated by AGN. According to the AKARI near-IR AGN diagnostics in Inami et al. (2018), LEDA1712304 is indeed classified as AGN-dominated galaxy; for AGNs, the near-IR flux density ratio, $F_{\nu}(4.3 \mu\text{m})/F_{\nu}(2.8 \mu\text{m})$, and the equivalent width of the PAH 3.3 μm feature, $EW(\text{PAH}_{3.3 \mu\text{m}})$, are expected to be > 1.0 and $< 0.06 \mu\text{m}$, respectively, while $F_{\nu}(4.3 \mu\text{m})/F_{\nu}(2.8 \mu\text{m})$ and the 3σ upper limit of $EW(\text{PAH}_{3.3 \mu\text{m}})$ are 7.5 ± 0.9 and $0.03 \mu\text{m}$, respectively, for LEDA 1712304, which is estimated by a Gaussian function with a local power-law continuum.

We evaluate the spectral properties through model fitting to the 2.5–12.5 μm spectrum. In previous studies with similar AGN modeling, for example, Sani et al. (2008) used a steep power-law continuum to reproduce a 3–5 μm spectrum, while Armus et al. (2007) used a hot-temperature blackbody with a cooler amorphous silicate absorption feature for a spectral range similar to ours. Referring to the latter, in reproducing the hot dust continuum and the deep spectral absorption feature, we assume a two-layer configuration for a dusty AGN torus, which is composed of a hot emitting inner layer and a warm absorbing outer layer. The hot emitting inner layer represents an optically thick hot dust layer which enshrouds the AGN core, while the warm absorbing outer layer represents a warm dust layer enveloping the hot inner layer. Hence the fitting function is described as

$$I_{\nu} = C_1 \exp(-N_{\text{dust}} \pi a^2 Q_{\text{abs},\nu} - \tau_{\text{CO}}) B_{\nu}(T_{\text{h}}), \quad (1)$$

where N_{dust} , a , $Q_{\text{abs},\nu}$, τ_{CO} and $B_{\nu}(T_{\text{h}})$ are the column density, the size, the absorption efficiency of silicate dust in the outer layer, the optical depth of the CO absorption feature and the Planck function with the temperature, T_{h} , of the hot dust emission from the optically thick inner layer, respectively. The dust size, a , is fixed at 0.1 μm , unless otherwise stated. For the CO gas absorption profile, we adopted a Gaussian function, the center of which was fixed at 4.67 μm .

As a first step, we assume the standard astronomical silicate (Draine 2003b) tentatively for the composition of dust in the absorbing outer layer. The fitted model is shown by a black line in the bottom panel of Fig. 1, while the fitting result is summarized in Table 2. We find that the standard astronomical silicate model does not reproduce the observed silicate absorption feature at all; not only the observed peak but also the feature profile is considerably different from those predicted by the model, as seen in the bottom panel of Fig. 1. In principle, the peak of the model feature can be shifted toward longer wavelengths by changing either the size or porosity of silicate dust (Laor & Draine 1993; Li et al. 2008). However we find that the feature profile of larger-size or porous astronomical silicate model then becomes too wide to reproduce the observed spectrum.

It is known that silicate features are fitted well with the composition of amorphous olivine ($\text{Mg}_{2x}\text{Fe}_{2-2x}\text{SiO}_4$; $x = 0.5$) rather than the astronomical silicate for heavily obscured AGNs

and Galactic center sources (Spoon et al. 2006; Kemper et al. 2004). Hence we test two kinds of models of amorphous olivine ($\text{Mg}_{2x}\text{Fe}_{2-2x}\text{SiO}_4$; $x = 0.5$ and 0.4 for models 2 and 3, respectively; Dorschner et al. 1995). The fitting results are listed in Table 2, which show that model 3 fits the spectrum better than model 2. The best-fit models of amorphous olivine ($x = 0.5$ and $x = 0.4$) are also shown in the bottom panel of Fig. 1, where we find that the feature profile is still not reproduced well by either model, although the peak wavelengths show better fits to the spectrum as compared to model 1.

Model 2 does not fit the spectrum very well at the bottom of the profile, while model 3 reproduces the bottom of the profile fairly well. In order to improve the former discrepancy, we add an absorption-free hot dust emission component in the model, which raises the floor level of the feature, as pointed out by Spoon et al. (2004). Thus the fitting function of equation (1) is modified as follows:

$$I_{\nu} = C_1 \exp(-N_{\text{dust}} \pi a^2 Q_{\text{abs},\nu} - \tau_{\text{CO}}) B_{\nu}(T_{\text{h}}) + C_2 B_{\nu}(T_{\text{h}}). \quad (2)$$

The result of the spectral fitting is shown by a green line in the bottom panel of Fig. 1 (model 4) and also in Table 2, where we find that model 4 improves the fit around the bottom of the profile and yet the fitting is still not acceptable on the basis of the χ^2 statistics. In particular, model 4 fails to reproduce the wing of the profile on the shorter wavelength side.

On the other hand, since model 3 predicts a feature profile narrower than the observed absorption feature, we change the porosity and size of amorphous olivine ($x = 0.4$) to widen the feature profile of model 3. We calculate the absorption efficiency of porous dust, averaging dielectric functions according to the Maxwell Garnett theory (Bohren & Huffman 1983). Assuming that the porosity of amorphous olivine ($x = 0.4$) is 30%, which is a volume fraction of the vacuum in a dust grain, we improve the fit to the silicate feature significantly (model 5; see the orange line in Fig. 1), except for the residual seen at around 9.3 μm . We also test a large-size silicate model (model 6), assuming 1 μm -sized amorphous olivine ($x = 0.4$), instead of the porous amorphous olivine. We however find that the fitting is only slightly improved from model 3 to model 6, and thus we conclude that the higher porosity is more favorable than the larger sizes for silicate grains.

Even with model 5, we find that there are systematic residuals at around 9.3 μm , which degrade the fitting near the bottom of the absorption profile significantly. Therefore we further add a crystalline pyroxene component (Jaeger et al. 1994) to the porous amorphous olivine component. Hence model 7 is a mixture of the porous amorphous olivine ($x = 0.4$) and crystalline pyroxene, which results in the best fitting among the silicate models we tested, as shown in Table 2.

3.2. Multi-wavelength photometric properties

Figure 2 shows the SED of LEDA 1712304, which is created with the flux densities listed in Table 1. We perform spectral decomposition using the four SED components of stellar, hot dust, warm dust and cold dust emission. We confirm that the photometric flux densities at 2.5–12.5 μm except that of the WISE 12 μm band which contains the silicate feature are consistent with the AKARI/IRC spectrum. We used the AKARI/IRC spectrum as well as the near- to mid-IR flux densities except the WISE 12 μm flux density for the SED fitting. As can be seen in Fig. 2, the SED exhibits that the UV to near-IR continuum is dominated by notably red stellar emission. Hence, in the SED fitting, we apply a stellar continuum model for an elliptical galaxy

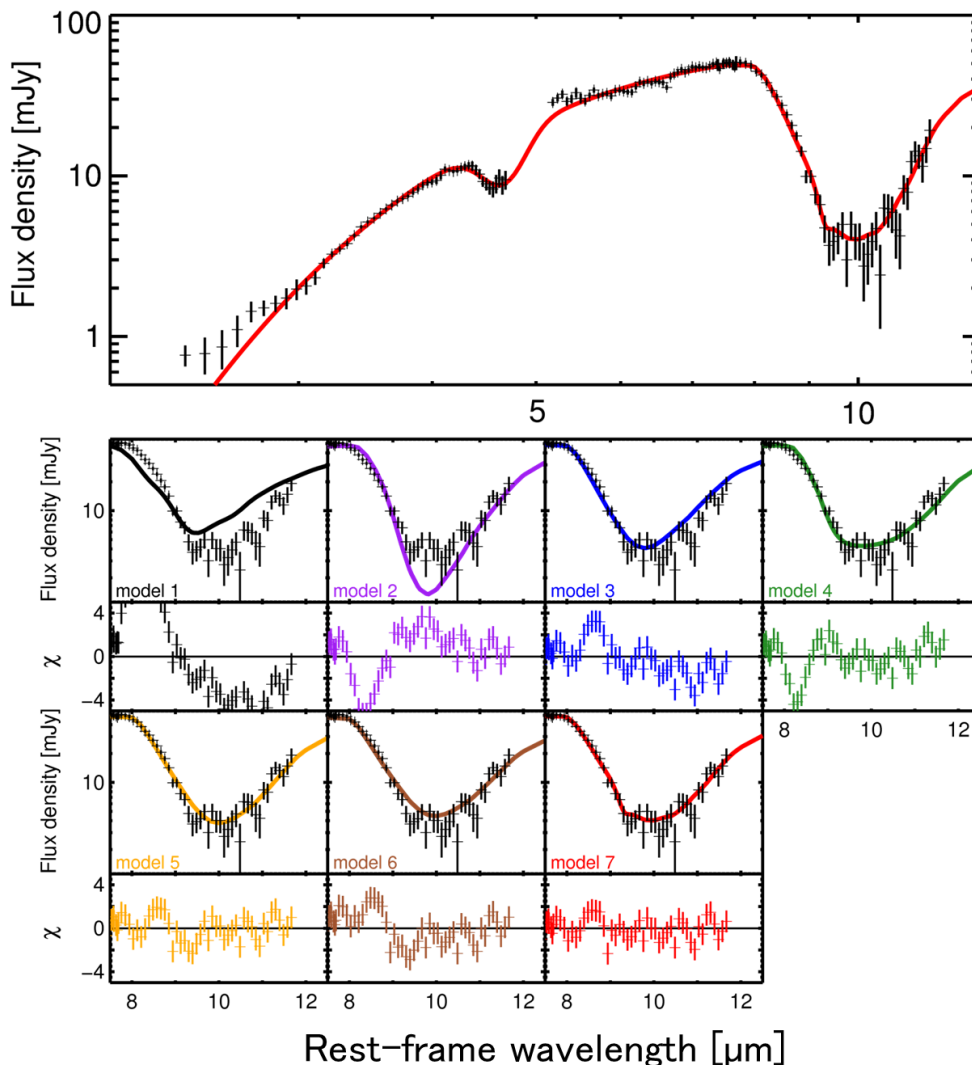


Fig. 1. *Top panel:* AKARI/IRC spectrum of LEDA 1712304 shown together with the best-fit model (model 7; red solid line). *Bottom panel:* A closed-up view of the fitting results of the $10\mu\text{m}$ silicate absorption feature with various spectral models and the residuals normalized by the errors. Black, purple, blue, green, orange, brown and red solid lines show the astronomical silicate (model 1), amorphous olivine ($\text{Mg}_{2x}\text{Fe}_{2-2x}\text{SiO}_4$, $x = 0.5$; model 2), amorphous olivine ($x = 0.4$; model 3), a combination of the amorphous olivine ($x = 0.5$) absorption and absorption-free emission component (model 4), the porous amorphous olivine ($x = 0.4$; model 5), the $1\mu\text{m}$ -sized amorphous olivine ($x = 0.4$; model 6) and a mixture of the porous amorphous olivine ($x = 0.4$) and the crystalline pyroxene (model 7), respectively.

(13 Gyr; Silva et al. 1998) and also take into account the reddening effect, for which the dust extinction law derived in Calzetti et al. (2000) is adopted. Since the near- to mid-IR range is dominated by hot dust emission, we adopt the best-fit silicate model derived from the spectral fitting (model 7) for the hot dust component. In the far-IR range, we find that double-temperature dust emission reproduces the SED fairly well. For the warm and cold dust components, we assume modified blackbody emission with the emissivity power-law index $\beta = 2$.

Based on the result of the SED fitting, we derive the stellar mass, M_{star} , the IR luminosity, L_{IR} , and the dust mass, M_{dust} , which are listed in Table 3. M_{star} is estimated by assuming the stellar-mass-to-luminosity ratio, $M_{\text{star}}/L_{K_s} \sim 1$ (Cole et al. 2001). L_{IR} is calculated to be $(5 \pm 1) \times 10^{10} L_{\odot}$ by integrating the best-fit model spectrum over the wavelength range of 8–1000 μm , which is consistent with the lower limit estimated by Hwang et al. (2013, $L_{\text{IR}} > 3.42 \times 10^{10} L_{\odot}$). The warm and cold

dust emission is likely to be optically thin in the far-IR range, and we can derive M_{dust} as

$$M_{\text{dust}} = \frac{F_{\nu} D^2}{B_{\nu}(T) \kappa_{\nu}}, \quad (3)$$

where F_{ν} , D , and κ_{ν} are the flux density, the distance to the galaxy and the mass absorption coefficient, respectively. κ_{ν} is assumed to be proportional to ν^2 , and we adopt $\kappa_{140\mu\text{m}} = 13.9 \text{ cm}^2/\text{g}$ (Draine 2003a). We also calculate the optical depth of the silicate feature, τ_{sil} , following the method defined by Imanishi et al. (2007), where an absorption-free continuum is assumed to be the power-law function determined from the flux densities at 7.1 and 14.2 μm . As a result, τ_{sil} is estimated to be 2.3 ± 0.2 at 9.8 μm , the wavelength of the bottom of the absorption feature.

We also performed the SED fitting of the heavily obscured AGN, using the bayesian-based SED fitting code CIGALE (Burgarella et al. 2005; Noll et al. 2009; Boquien et al. 2019) which

Table 2. Summary of the results of the IR spectral fitting with various silicate dust models.

model	composition	χ^2/dof^a	porosity	T_h [K]	N_{dust} [10^{11} cm^{-2}]
1	astronomical silicate	24.5	–	486 ± 2	0.573 ± 0.007
2	amorphous olivine ($x = 0.5$)	6.4	–	495 ± 1	1.02 ± 0.02
3	amorphous olivine ($x = 0.4$)	3.4	–	500 ± 1	0.95 ± 0.01
4	amorphous olivine ($x = 0.5$) + absorption-free continuum	3.1	–	494 ± 1	1.36 ± 0.04
5	porous amorphous olivine ($x = 0.4$)	1.6	0.3	502 ± 1	1.06 ± 0.01
6	$1 \mu\text{m}$ -sized amorphous olivine ($x = 0.4$)	2.7	–	552 ± 1	0.080 ± 0.001
7	96% porous amorphous olivine ($x = 0.4$) + 4% crystalline pyroxene (96:4)	1.2	0.3	493 ± 1	1.05 ± 0.01

Notes. ^(a) χ^2 is calculated for the rest-frame spectral range of 8–12 μm . The degree of freedom (dof) is 35.

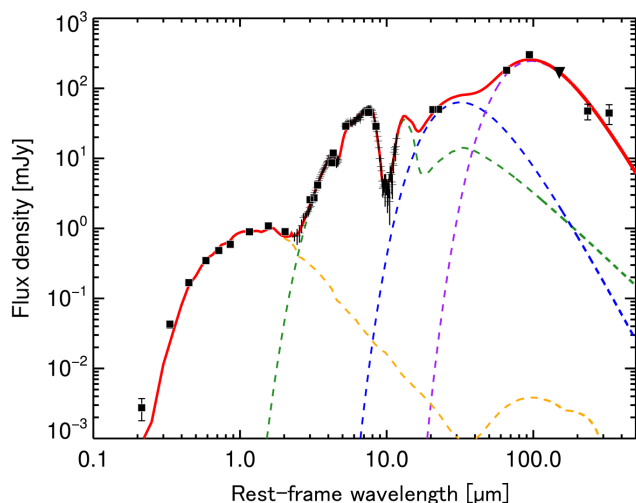


Fig. 2. Spectral energy distribution of LEDA 1712304. Filled squares correspond to the observed flux densities, while a downward triangle represents the 3σ upper limit. The AKARI/IRC spectral data at 2.5–12.5 μm are also included in the fitting. A red solid line shows the best-fit model, where the stellar, hot dust, warm dust and cold dust components are shown by yellow, green, blue and purple dashed lines, respectively.

includes energy balance between the dust absorption of the stellar/AGN emission and the dust re-emission in the mid/far-IR, similarly to the study by Ciesla et al. (2015). As a result, M_{star} and L_{IR} , are estimated to be $8 \times 10^9 M_{\odot}$ and $6 \times 10^{10} L_{\odot}$, respectively. Comparing the result in Table 3, we find that M_{star} increases while L_{IR} does not change. The increase in M_{star} , however, does not change our conclusion below.

4. Discussion

4.1. Comparison with other AGNs

We detect a deep ($\tau_{\text{sil}} \sim 2.3$) absorption feature due to silicate grains at around 10 μm . We compare the optical depth of the silicate feature in LEDA 1712304 with those in other AGNs in a wide range of IR luminosities ($10^{10} L_{\odot} < L_{\text{IR}} < 10^{13} L_{\odot}$). The spectra of the AGNs to be compared are taken from those of the IR galaxy samples observed by *Spitzer*/IRS (Stierwalt et al. 2013; Imanishi et al. 2007; Imanishi 2009; Roussel et al. 2006) with the threshold that the equivalent width of the PAH 6.2 μm feature is smaller than 0.27 μm (Stierwalt et al. 2013). In addition,

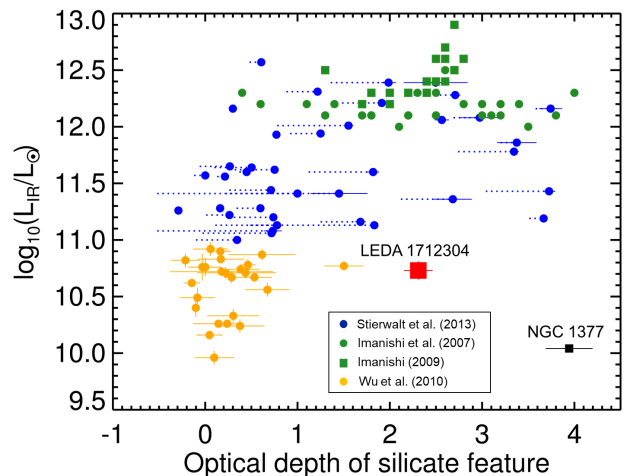


Fig. 3. Relation between the IR luminosity and the optical depth of the silicate feature for LEDA 1712304 and other AGN samples (Stierwalt et al. 2013; Imanishi et al. 2007; Imanishi 2009; Roussel et al. 2006; Wu et al. 2010). Red and black squares represent LEDA 1712304 and NGC 1377 (Roussel et al. 2006), respectively. Blue, green, orange circles and green squares represent the AGN samples of Stierwalt et al. (2013), Imanishi et al. (2007), Wu et al. (2010) and Imanishi (2009), respectively. We use the IR luminosities obtained in each reference paper. We estimate the optical depth of the silicate feature for LEDA 1712304 and the AGN samples of Stierwalt et al. (2013), Wu et al. (2010) and Roussel et al. (2006) by ourselves, using the method defined by Imanishi et al. (2007), while we take the values in each reference paper for the other AGNs. We also show the differences between our estimates and those by Stierwalt et al. (2013) with the blue dotted horizontal lines.

tion, we also take AGN samples with low IR luminosities ($L_{\text{IR}} < 10^{11} L_{\odot}$) from Wu et al. (2010). Figure 3 shows the relation between the IR luminosity and the optical depth of the silicate feature for LEDA 1712304 and the AGN samples. We estimate the optical depths of the AGN samples of Stierwalt et al. (2013), Wu et al. (2010) and Roussel et al. (2006) by ourselves in the same manner as performed for LEDA 1712304, with the method defined by Imanishi et al. (2007), the spectra of which are obtained from the NASA/IPAC IR Science Archive (IRSA). On the other hand, we adopt the values given in each reference paper for the other AGNs. The blue dotted lines in Fig. 3 show the differences between our estimates and those by Stierwalt et al. (2013), from which we confirm that the differences between the different methods are not as large as to change a global relation. Fig. 3 exhibits that galaxies with low IR luminosities ($L_{\text{IR}} < 10^{11} L_{\odot}$) show significantly shallow silicate absorption features as already

Table 3. Luminosities and masses of LEDA 1712304 obtained with the SED fitting.

$L_{\text{IR}} [L_{\odot}]$	$L_{\text{hot}} [L_{\odot}]$	$L_{\text{warm}} [L_{\odot}]$	$L_{\text{cold}} [L_{\odot}]$
$(5 \pm 1) \times 10^{10}$	$(4.20 \pm 0.06) \times 10^{10}$	$(1.8 \pm 0.8) \times 10^{10}$	$(2.3 \pm 0.6) \times 10^{10}$
$M_{\text{star}} [M_{\odot}]^a$	$M_{\text{dust,w}} [M_{\odot}]$	$M_{\text{dust,c}} [M_{\odot}]$	
$(2.7 \pm 0.8) \times 10^9$	$(1.1 \pm 0.5) \times 10^4$	$(1.1 \pm 0.3) \times 10^7$	

Notes. ^(a) The uncertainty corresponds to that in the adopted initial mass function (Cole et al. 2001).

pointed out by Stierwalt et al. (2013). Imanishi (2009) suggested that the number of heavily obscured AGNs which have deep silicate absorption features ($\tau_{\text{sil}} > 2$) increases with the IR luminosities of the host galaxies. Therefore LEDA 1712304 may be a rare galaxy from the aspect of having both deep absorption feature $\tau_{\text{sil}} \sim 2.3$ and low IR luminosity $(5 \pm 1) \times 10^{10} L_{\odot}$. Indeed, such galaxies have hardly been observed; an exception is NGC 1377 (Roussel et al. 2006), as can be seen in Fig. 3. NGC 1377 is a lenticular galaxy (de Vaucouleurs et al. 1991), the stellar mass of which is $10^{9.3 \pm 0.1} M_{\odot}$ (Skibba et al. 2011). The IR spectrum of NGC 1377 shows a featureless continuum except the silicate feature due to circumnuclear dust (Imanishi 2006; Roussel et al. 2006).

The low IR luminosity reflects a relatively low star formation rate (SFR) in LEDA 1712304. We applied the cold dust luminosity L_{cold} in Table 3 instead of L_{IR} to estimate the SFR, since L_{IR} is likely to be contaminated with the AGN activity. The resultant SFR is $4 M_{\odot}/\text{yr}$, based on the L_{IR} -SFR relation in Kennicutt & Evans (2012). Hence the star formation is not active in the host galaxy, which is also expected from non-detection of the PAH features as well as the stellar continuum model of an elliptical galaxy for the SED fitting. Kauffmann et al. (2003) reported that the stellar masses of AGN host galaxies range from $10^{9.5} M_{\odot}$ to $10^{12} M_{\odot}$ based on the SDSS survey, whereas LEDA 1712304 has $M_{\text{star}} = (2.7 \pm 0.8) \times 10^9 M_{\odot}$ (or $8 \times 10^9 M_{\odot}$ from the CIGALE fitting; see Section 3.2). Therefore LEDA 1712304 belongs to the population of a considerably low mass class which harbors an AGN. Thus the host galaxy is expected to be an early-type galaxy of low mass classes and yet possesses a heavily observed AGN; LEDA 1712304 is likely to belong to a population missed in the previous observations, and aforementioned NGC 1377 may be in an evolutionary stage similar to LEDA 1712304.

In Figure 4, we compare the silicate feature profile of LEDA 1712304 with those of the other AGNs, classifying them with L_{IR} . Fig. 4 shows that more AGN samples in a lower L_{IR} class tend to have shallower silicate absorption features ($\tau_{\text{sil}} < 1$), which is consistent with the trend in Fig. 3. Fig. 4 also shows that the spectra of many AGN samples exhibit strong emission features, such as PAH $7.7 \mu\text{m}$, $8.6 \mu\text{m}$, $11.3 \mu\text{m}$, $\text{H}_2 \text{ S}(3)$ $9.66 \mu\text{m}$ and $[\text{S IV}]$ $10.5 \mu\text{m}$, in the wavelength range containing the silicate feature. On the other hand, LEDA 1712304 has one of the most featureless continua except the silicate features in the AGN samples, and thus is expected to be one of the purest AGN-dominated galaxy in the AGN samples. In Fig. 5, for the purpose of investigating difference, if any, in the absorption profile, we also show the optical depth profiles of the silicate features for only the AGN samples with deep silicate absorption features ($\tau_{\text{sil}} > 2$), which are normalized by the optical depths averaged over the wavelength range of 9.8 – $10.3 \mu\text{m}$ that include no strong lines. Fig. 5 shows that the silicate absorption profiles thus normalized are notably similar from galaxy to galaxy, although their L_{IR} values are much different. And yet we find that the wings of the profiles vary on the shorter wavelength side. At around $9 \mu\text{m}$, the wing of LEDA 1712304 is shifted significantly toward

longer wavelengths than those of many other AGNs, especially those with $L_{\text{IR}} < 10^{12} L_{\odot}$, which can be explained by differences in the compositions of amorphous olivine (e.g., the difference between models 2 and 3, see the bottom panel in Fig. 1) and/or the crystallinity (the difference between models 3 and 7).

The above variations at around $9 \mu\text{m}$ could be produced by the PAH 7.7 and $8.6 \mu\text{m}$ features filling the silicate absorption. Since the galaxies are located at various distances, the spectroscopic apertures do not sample the same physical scales of the nuclei and thus the PAH emission from host galaxies with larger distances is expected to contaminate the spectra more strongly. We explore this possibility in Fig. 6, where the variations at around $9 \mu\text{m}$ are plotted as a function of the redshift. In the figure, the contamination of the PAH features from host galaxies would produce a decreasing trend with the redshift. However, Fig. 6 does not show any clear dependence on the distance and therefore we conclude that the aperture effects with the different distances do not make an appreciable contribution to the variations of the silicate absorption profiles.

4.2. Silicate dust properties in LEDA 1712304

Such a deep silicate absorption calls for the presence of a strong dust temperature gradient (Imanishi et al. 2007), since both absorber and emitter in the mid-IR are of dust origin; the absorbing silicate dust is considered as cooler dust in the outer region of the AGN torus or interstellar dust in the host galaxy, while the strong continuum emission at around $10 \mu\text{m}$ is attributed to hotter dust close to the AGN core. Here we consider the possibility that the absorbing dust is of interstellar origin in LEDA 1712304. As shown in Table 2, we estimated the column density of the absorbing dust with the spectral fitting, from which we calculate the whole mass of the silicate dust assuming the size of the galaxy, ~ 15 kpc (SDSS DR6; Adelman-McCarthy et al. 2008)¹, as the size of the absorbing dust layer. The resultant silicate dust mass is $9 \times 10^8 M_{\odot}$, which is much larger than the warm and cold dust masses in Table 3. On the other hand, assuming that the size of the absorbing dust layer is 100 pc, typical of a circumnuclear dusty torus, the silicate dust mass is estimated to be $4 \times 10^4 M_{\odot}$, which is reasonable as compared with the warm dust mass in Table 3. Therefore the absorbing silicate dust is likely of not interstellar but circumnuclear origin, which is present in the outer region of the AGN torus.

The silicate feature of the AGN torus dust in LEDA 1712304 is different in the profile from that of the astronomical silicate. The result of the IR spectral fitting indicates that the difference in the silicate features is attributed to either composition, the physical structure of dust, or both. The best-fit model (model 7) needs amorphous olivine as a dominant composition, which is consistent with the result of Spoon et al. (2006) for heavily obscured ULIRG nuclei. Based on the fact that the main compo-

¹ The size of LEDA 1712304 is estimated by averaging the isophotal radii of the major and minor axes in the SDSS r band image.

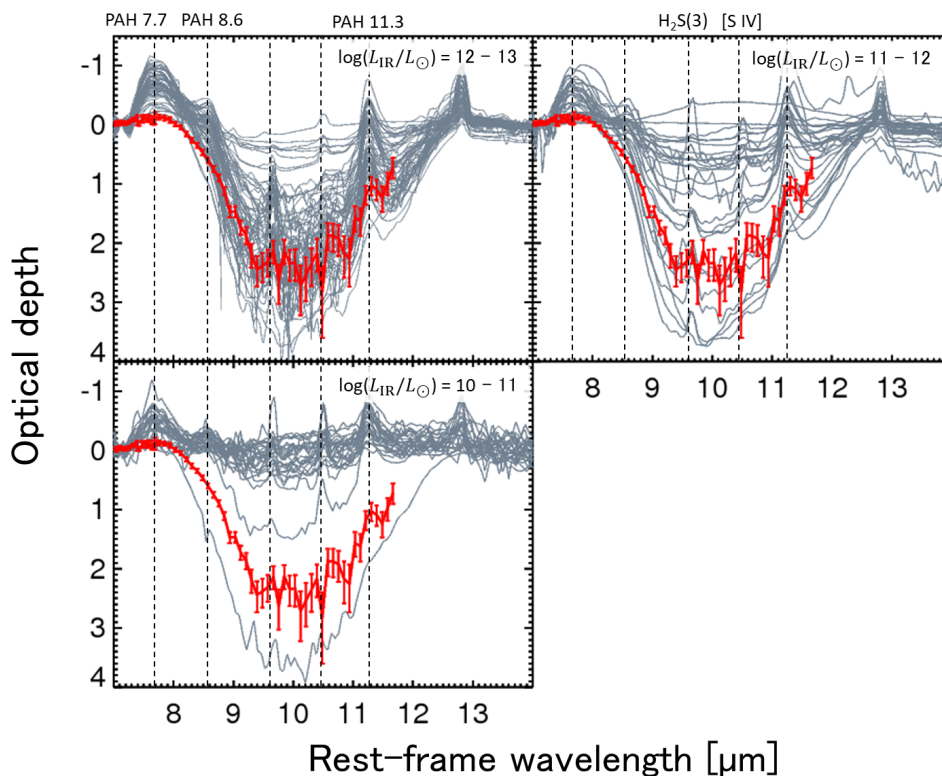


Fig. 4. Optical depth profiles of the silicate features for LEDA 1712304 (red) and the other AGN samples (grey; Stierwalt et al. 2013; Imanishi et al. 2007; Imanishi 2009; Roussel et al. 2006; Wu et al. 2010). *Top right, top left and bottom panels* show the optical depth profiles of the AGN samples in the IR luminosity ranges of 10^{12} – $10^{13} L_{\odot}$, 10^{11} – $10^{12} L_{\odot}$ and 10^{10} – $10^{11} L_{\odot}$, respectively. Each optical depth profile is obtained by the absorption-free power-law continuum determined from the flux densities at $7.1 \mu\text{m}$ and $14.2 \mu\text{m}$ (Imanishi et al. 2007). The dashed lines show the positions of PAH 7.7, 8.6 and $11.3 \mu\text{m}$, $\text{H}_2\text{S}(3)$ $9.66 \mu\text{m}$ and $[\text{S IV}]$ $10.5 \mu\text{m}$.

sition of dust in the circumstellar dust shells around late M stars is also amorphous olivine (Roche et al. 2007), we speculate that the grains of amorphous olivine generated in the old stars may have fallen into the galactic center as induced by a galaxy interaction, for example, which can explain amorphous-olivine rich dusty torus around the AGN.

Spoon et al. (2004) suggested the presence of an unobscured emission component to explain the flat spectrum at the bottom of the silicate feature of a heavily obscured AGN. Indeed, the model which considers an absorption-free continuum (model 4) gives a better fit to the spectrum of LEDA 1712304 than that which only considers the obscured circumnuclear hot dust (model 2). On the other hand, the even better-fit result of the IR spectral fitting is the porous amorphous olivine (model 5 and 7). The porosity of the silicate dust may be caused by coagulations or processing in the circumnuclear environments. The result of the IR spectral fitting also suggests that the dusty torus around the AGN in LEDA 1712304 is likely to contain the crystalline silicate. Kemper et al. (2004) reported that the crystallinity of the diffuse interstellar silicate dust in our Galaxy is smaller than 2.2% and the absence of crystalline silicate is explained by an amorphization process caused by cosmic-ray particle bombardment which occurs on a timescale significantly shorter than the destruction timescale. The crystallinity of silicate dust in the AGN torus in LEDA 1712304 is $\sim 4\%$ from the IR spectral fitting, which is larger than that of the diffuse interstellar dust in our Galaxy. Therefore the silicate dust in the AGN torus in LEDA 1712304 is likely to be relatively fresh, possibly formed in the circumnuclear dense environments.

5. Conclusions

We detect a deep ($\tau_{\text{sil}} \sim 2.3$) absorption feature due to silicate grains at around $10 \mu\text{m}$ in the AKARI/IRC near- to mid-IR spectrum of the nearby heavily obscured galaxy LEDA 1712304. The spectrum also shows a steep near- to mid-IR slope, indicating that LEDA 1712304 possesses a heavily obscured AGN. The IR luminosity and stellar mass of LEDA 1712304, $L_{\text{IR}} = (5 \pm 1) \times 10^{10} L_{\odot}$ and $M_{\text{star}} = (2.7 \pm 0.8) \times 10^9 M_{\odot}$, are notably low compared with other heavily obscured AGNs which show deep silicate absorptions. Thus LEDA 1712304 may be a rare galaxy showing low L_{IR} , low M_{star} and yet large τ_{sil} . On the other hand, we find that the spectral profile of the silicate feature in LEDA 1712304 is similar to those of the other AGN samples as a whole, but significantly different in the wing on the shorter wavelength side, which can be explained by difference in the compositions and/or the crystallinity.

The absorbing silicate dust in LEDA 1712304 is not of interstellar origin but of circumnuclear origin, since the dust mass estimated from τ_{sil} and the size of host galaxy is much larger than that estimated from the far-IR emission. From the IR spectral fitting, the main composition of the circumnuclear silicate dust in LEDA 1712304 is amorphous olivine, which is consistent with the previous studies (e.g., Spoon et al. 2006). In addition, the best-fit model of the IR spectral fitting calls for the porosity and the crystallinity of the silicate dust, which imply the dust coagulation or processing and recent dust formation, respectively, in the circumnuclear environments.

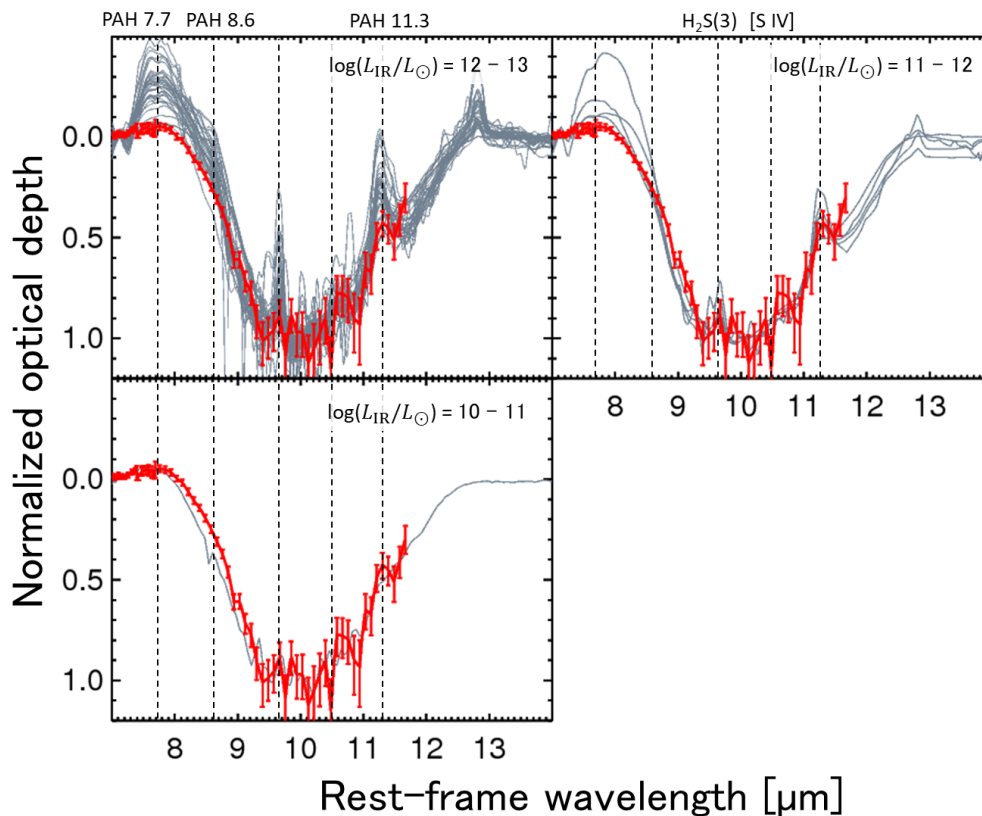


Fig. 5. Normalized optical depth profiles of the silicate features for LEDA 1712304 (red) and the other AGN samples (grey; Stierwalt et al. 2013; Imanishi et al. 2007; Imanishi 2009; Roussel et al. 2006) which have deep silicate absorption features ($\tau_{\text{sil}} > 2$). The normalization is performed by the mean optical depths at the wavelength range of 9.8–10.3 μm which include no strong lines. The dashed lines show the positions of PAH 7.7, 8.6 and 11.3 μm , H₂ S(3) 9.66 μm and [S IV] 10.5 μm .

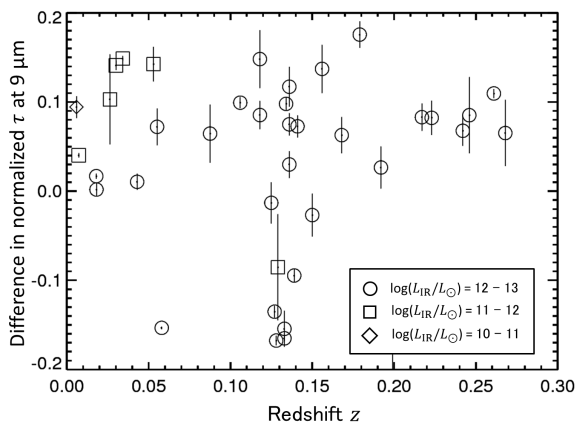


Fig. 6. Difference in the normalized optical depth at around 9 μm from that of LEDA 171304 as a function of the redshift, which is calculated by averaging the differences at 8.9–9.1 μm . A larger value indicates a deeper silicate feature at around 9 μm . Circles, squares and diamonds correspond to the galaxies with $L_{\text{IR}} = 10^{12}$ – $10^{13} L_{\odot}$, 10^{11} – $10^{12} L_{\odot}$ and 10^{10} – $10^{11} L_{\odot}$, respectively.

Acknowledgements. We thank the referee for carefully reading our manuscript and giving us helpful comments. This work is based on observations with AKARI, a JAXA project with the participation of ESA, with the Spitzer Space Telescope, which is operated by the Jet Propulsion Laboratory, California Institute of Technology under a contract with NASA, using the NASA/IPAC Infrared Science Archive and with *Herschel*, which is an ESA space observatory with sci-

ence instruments provided by European-led Principal Investigator consortia and with important participation from NASA. The IRSF project was financially supported by the Sumitomo foundation and Grants-in-Aid for Scientific Research on Priority Areas (A) (Nos. 10147207 and 10147214) from the Ministry of Education, Culture, Sports, Science and Technology (MEXT). The operation of IRSF is supported by Joint Development Research of National Astronomical Observatory of Japan, and Optical Near-Infrared Astronomy Inter-University Cooperation Program, funded by the MEXT of Japan.

References

- Adelman-McCarthy, J. K., Agüeros, M. A., Allam, S. S., et al. 2008, *ApJS*, 175, 297
- Antonucci, R. 1993, *ARA&A*, 31, 473
- Armus, L., Charmandaris, V., Bernard-Salas, J., et al. 2007, *ApJ*, 656, 148
- Bohren, C. F. & Huffman, D. R. 1983, *Absorption and scattering of light by small particles*
- Boquien, M., Burgarella, D., Roehlly, Y., et al. 2019, *A&A*, 622, A103
- Burgarella, D., Buat, V., & Iglesias-Páramo, J. 2005, *MNRAS*, 360, 1413
- Calzetti, D., Armus, L., Bohlin, R. C., et al. 2000, *ApJ*, 533, 682
- Ciesla, L., Charmandaris, V., Georgakakis, A., et al. 2015, *A&A*, 576, A10
- Cole, S., Norberg, P., Baugh, C. M., et al. 2001, *MNRAS*, 326, 255
- Cutri, R. M., Skrutskie, M. F., van Dyk, S., et al. 2003, *VizieR Online Data Catalog*, 2246
- Cutri, R. M., Wright, E. L., Conrow, T., et al. 2013, *Explanatory Supplement to the ALLWISE Data Release Products*, Tech. rep.
- de Vaucouleurs, G., de Vaucouleurs, A., Corwin, Jr., H. G., et al. 1991, *Third Reference Catalogue of Bright Galaxies. Volume I: Explanations and references. Volume II: Data for galaxies between 0^h and 12^h. Volume III: Data for galaxies between 12^h and 24^h*
- Dey, A., Soifer, B. T., Desai, V., et al. 2008, *ApJ*, 677, 943
- Dorschner, J., Begemann, B., Henning, T., Jaeger, C., & Mutschke, H. 1995, *A&A*, 300, 503

- Draine, B. T. 2003a, *ARA&A*, 41, 241
- Draine, B. T. 2003b, *ApJ*, 598, 1026
- Fazio, G. G., Hora, J. L., Allen, L. E., et al. 2004, *ApJS*, 154, 10
- Griffin, M. J., Abergel, A., Abreu, A., et al. 2010, *A&A*, 518, L3
- Hao, L., Weedman, D. W., Spoon, H. W. W., et al. 2007, *ApJ*, 655, L77
- Hwang, H. S., Andrews, S. M., & Geller, M. J. 2013, *ApJ*, 777, 38
- Imanishi, M. 2006, *AJ*, 131, 2406
- Imanishi, M. 2009, *ApJ*, 694, 751
- Imanishi, M., Dudley, C. C., Maiolino, R., et al. 2007, *ApJS*, 171, 72
- Imanishi, M., Nakagawa, T., Ohyama, Y., et al. 2008, *PASJ*, 60, S489
- Inami, H., Armus, L., Matsuhara, H., et al. 2018, *A&A*, 617, A130
- Jaeger, C., Mutschke, H., Begemann, B., Dorschner, J., & Henning, T. 1994, *A&A*, 292, 641
- Kauffmann, G., Heckman, T. M., Tremonti, C., et al. 2003, *MNRAS*, 346, 1055
- Kemper, F., Vriend, W. J., & Tielens, A. G. G. M. 2004, *ApJ*, 609, 826
- Kennicutt, R. C. & Evans, N. J. 2012, *ARA&A*, 50, 531
- Laor, A. & Draine, B. T. 1993, *ApJ*, 402, 441
- Li, M. P., Shi, Q. J., & Li, A. 2008, *MNRAS*, 391, L49
- Lutz, D., Spoon, H. W. W., Rigopoulou, D., Moorwood, A. F. M., & Genzel, R. 1998, *ApJ*, 505, L103
- Murakami, H., Baba, H., Barthel, P., et al. 2007, *PASJ*, 59, S369
- Nagashima, C., Nagayama, T., Nakajima, Y., et al. 1999, in *Star Formation 1999*, ed. T. Nakamoto, 397–398
- Nagayama, T., Nagashima, C., Nakajima, Y., et al. 2003, in *Proc. SPIE, Vol. 4841, Instrument Design and Performance for Optical/Infrared Ground-based Telescopes*, ed. M. Iye & A. F. M. Moorwood, 459–464
- Noll, S., Burgarella, D., Giovannoli, E., et al. 2009, *A&A*, 507, 1793
- Ohyama, Y., Onaka, T., Matsuhara, H., et al. 2007, *PASJ*, 59, S411
- Onaka, T., Matsuhara, H., Wada, T., et al. 2007, *PASJ*, 59, S401
- Oyabu, S., Ishihara, D., Malkan, M., et al. 2011, *A&A*, 529, A122
- Poglitsch, A., Waelkens, C., Geis, N., et al. 2010, *A&A*, 518, L2
- Rieke, G. H., Young, E. T., Engelbracht, C. W., et al. 2004, *ApJS*, 154, 25
- Roche, P. F., Aitken, D. K., Smith, C. H., & James, S. D. 1986, *MNRAS*, 218, 19P
- Roche, P. F., Alonso-Herrero, A., & Gonzalez-Martin, O. 2015, *MNRAS*, 449, 2598
- Roche, P. F., Packham, C., Aitken, D. K., & Mason, R. E. 2007, *MNRAS*, 375, 99
- Roussel, H., Helou, G., Smith, J. D., et al. 2006, *ApJ*, 646, 841
- Sanders, D. B. & Mirabel, I. F. 1996, *Annual Review of Astronomy and Astrophysics*, 34, 749
- Sani, E., Risaliti, G., Salvati, M., et al. 2008, *ApJ*, 675, 96
- Silva, L., Granato, G. L., Bressan, A., & Danese, L. 1998, *ApJ*, 509, 103
- Skibba, R. A., Engelbracht, C. W., Dale, D., et al. 2011, *ApJ*, 738, 89
- Spoon, H. W. W., Armus, L., Cami, J., et al. 2004, *ApJS*, 154, 184
- Spoon, H. W. W., Marshall, J. A., Houck, J. R., et al. 2007, *ApJ*, 654, L49
- Spoon, H. W. W., Tielens, A. G. G. M., Armus, L., et al. 2006, *ApJ*, 638, 759
- Stierwalt, S., Armus, L., Charmandaris, V., et al. 2014, *ApJ*, 790, 124
- Stierwalt, S., Armus, L., Surace, J. A., et al. 2013, *ApJS*, 206, 1
- Urry, C. M. & Padovani, P. 1995, *PASP*, 107, 803
- Wu, Y., Helou, G., Armus, L., et al. 2010, *ApJ*, 723, 895
- Yamagishi, M., Yamamura, I., Mizuki, T., et al. 2019, *PASJ*, 71, 3